Supporting Information

Beer et al. 10.1073/pnas.1714085115

SI Materials and Methods

Worm Strains and Maintenance. Maternal-zygotic *bec-1* and *vps-34* mutant embryos were isolated as described (1). As *vps-34* mutants arrest as larvae, they are rescued by an extrachromosomal array carrying a wild-type copy of the *vps-34* gene. Although these arrays are typically silenced in the germ line and early embryo, weak/occasional maternal transcription from the rescuing array is likely responsible for the weaker phenotypes of *vps-34* mutants compared with *bec-1* mutants.

Plasmid Construction. sgRNA plasmids were amplified from pDD122 with the sgRNA primers below in addition to the pDD122 sgRNA R primer by using the Q5 site-directed mutagenesis kit (New England Biolabs) according to Dickinson et al. (2). The *pie-1::GFP::ZF1::PH* plasmid was constructed by moving the PH domain of rat PLCδ1 from the PH entry vector pJN415 to the *pie-1::GFP::ZF1::Gateway* destination vector pJN371 using Gateway cloning (Invitrogen). To construct pGF07 (*pie-1::mCh::PH::ZF1*), the sequence of the PH domain of rat PLCδ1 and the ZF1 domain of *pie-1* was codon-optimized by using the *C. elegans* codon adaptor (3) and ordered from Eurofins Genomics to create plasmid pEX-A2-*PH::ZF1*. PH:ZF1 was amplified from pEX-A2-*PH::ZF1* by using a two-step PCR with primers attB ATG coPH and attB Stop coZF1 followed by primers attB1 and attB2 and cloned into pDonr221 (Invitrogen) to generate *PH::ZF1* entry clone pGF06. PH::ZF1 was then moved into pAZ132-*mCh::Gateway* destination vector (gift of Barth Grant, Rutgers University, Piscataway, NJ) to generate pGF07. The *pie-1::mCh::UNC-108* plasmid pGF14 was constructed by amplifying *unc-108* from pSD17 (gift of Michael Ailion, University of Washington, Seattle) using a two-step PCR with attB ATG *rab-2* and attB STOP *rab-2* primers, followed by attB1 and attB2 primers. The construct was introduced into the pDonr221 entry vector and then moved into pAZ132-*mCh::Gateway* destination vector to generate pGF14. The *pie-1::mCh::2xFYVE* plasmid was constructed by amplifying two tandem FYVE domains of EEA-1 from the plasmid pRA017 (gift of Julie Ahringer, Gurdon Institute, Cambridge, UK) using a two-step PCR with primers attB MCS 2xFYVE and attB Stop 2xFYVE, followed by attB1 and attB2 primers. By using Gateway cloning, the PCR was introduced into pDonor221 and pAZ132-*mCh::Gateway*. For the *rme-8* RNAi plasmid, the *rme-8* primers were used to clone a 1-kb fragment of *rme-8* from cDNA into pPD129.36 using TA cloning. The resulting plasmid was transformed into HT115 bacteria for RNAi experiments. Primer sequences are given in Table S3.

CRISPR/Cas9-Mediated Genome Editing. The *pad-1* deletion allele *wur02* was obtained by injecting three Cas9 + sgRNA plasmids (ATG2, Stop1, and Stop6) as well as the pRF4[*rol-6(su1006d)*] marker to delete 24 kb of *pad-1* genomic sequence (4). A 23.5-kb deletion was verified by sequencing and includes the following 21-bp insertion (capital letters) between the break sites (lowercase):

ttgcagaaagaaataagaaatggcatcagcGTGGATTAGGCATCAG-CGTGGcgtggatttttctgaacatttgcaatttta. Thus, only 12 aa of the 2,417-aa PAD-1 protein are predicted to remain in the *wur02* allele. The heterozygous deletion strain was crossed with WEH126 to balance the sterile mutant and generate the WEH159 strain.

The GFP::PAD-1 strain MCP6 was generated by Maïté Carre-Pierrat, University of Lyon, Lyon, France using CRISPR/Cas9 to knock eGFP with introns into the N terminus of PAD-1 (4). N2 worms were injected with *pad-1* ATG sgRNA2 and a PCR repair template amplified from pPD95.75 with the nested primers oMCP039F, oMCP040R, and oMCP041R. Correct insertion of GFP was verified by sequencing. The MCP6 strain was fertile and viable, unlike *pad-1* deletion mutants, indicating that GFP::PAD-1 is functional.

Worm Transformation. Transgenic strains were made by biolistic transformation (Bio-Rad PDS 1000) of the HT1593 strain by standard methods (5). The FT1091 strain was generated by bombardment with *pie-1p::GFP::ZF1::PH* plasmid, WEH260 with *pGF7*, WEH315 with *pGF14*, and WEH327 with *pie-1p::mCh::2xFYVE*. The WEH14 strain was generated by bombardment with the following GFP-tagged fosmid from the TransgenOme project (6): WRM06_12A_D10(pRedFlp-Hgr) (F11A10.4[28269]::S0001_pR6K_Amp_2xTY1ce_EGFP_FRT_rpsl_neo_FRT_3xFlag) dFRT::unc-119-Nat. To verify that the MON-2::GFP reporter was functional, WEH14 was crossed into the *mon-2* mutant strain XH2006 to generate the strain WEH244. WEH244 was stained with mouse anti–LMP-1 antibody, and the size of the LMP-1-positive vesicles was examined. LMP-1-positive late endosomes or lysosomes were not enlarged in WEH244 (Fig. S5*E*), indicating that MON-2::GFP is functional.

Knockdown by RNAi. RNAi was performed by feeding L1 larvae through adulthood at 25 °C, as described (7). Control worms were fed with the empty RNAi vector pPD129.36 in HT115 bacteria. For *rme-8* RNAi, worms were treated starting at the L3 stage to avoid sterility or larval lethality. For RNAi of the Cdc50 family proteins, *chat-1(ok1681)* adults were injected with 1 μg/μL F20C5.4 and W03G11.2 dsRNA (transcribed in vitro from T7 PCRs) and incubated at room temperature for >24 h before staining maternal zygotic mutant embryos. The following RNAi clones were used from available libraries (Source BioScience): *pad-1* (JA:Y18D10A.13), *tat-5* (JA:F36H2.1), *mon-2* (JA:F11A10.4), *vps-26* (JA:T20D3.7), *vps-29* (JA:ZK1128.8 and MV:ZK1128.8), *vps-35* (JA:F59G1.3), *snx-1* (MV:C05D9.1), *snx-3* (JA:W06D4.5), *snx-6* (MV:Y59A8B.22), *lst-4* (JA:Y37A1B.2 and MV:Y37A1B.2), F20C5.4 (JA:F20C5.4 and MV:F20C5.4), and W03G11.2 (MV:W03G11.2).

Light Microscopy. Most fluorescent images were taken on a Leica DM5500 wide-field fluorescence microscope with a HC PL APO 40× 1.3-NA oil objective or a HCX PL APO 63× 1.4-NA glycerol objective with a Leica DFC365 FX CCD camera controlled by LAS AF software. Live colocalization images in Fig. S6 were collected simultaneously on a Leica SP8 confocal with a HC PL APO CS2 63× 1.2-NA water objective with HyD detectors.

Electron Microscopy. Electron micrographs were obtained from high-pressure frozen, freeze-substituted, gravid adults, as described (8, 9). Tilt series were also collected on a 200-kV JEM-2100 transmission electron microscope (JEOL) equipped with a TemCam F416 4k × 4k camera (Tietz Video and Imaging Processing Systems) running Serial EM software (10). Tomograms were computed by using eTomo and IMOD software (11).

Antibody Staining. Embryos were freeze-fractured, fixed in methanol or methanol plus paraformaldehyde, and stained as described (1). Fluorescent secondary antibodies were obtained from Jackson ImmunoResearch, and the following primary antibodies were used: chicken α-GFP (Aves), chicken α-GFP (Chemicon), rabbit α-GFP (Abcam), Living Colors rabbit α-DsRed (Clontech), rabbit α-SYX-4 [gift of Michael Glotzer, University of Chicago, Chicago (12)], rabbit α-EEA-1 [gift of Barth Grant (13)], rabbit α-RME-8 [gift of Barth Grant (14)], rabbit α-HGRS-1 [gift of

Renaud Legouis, University Paris-Saclay, Gif-sur-Yvette, France (15)], and rabbit α-VPS-32 [gift of Renaud Legouis (16)], as well as mouse α-APA-2, α-CAV-1, α-LMP-1, α-RME-1, and α-SQV-8 from the Developmental Studies Hybridoma Bank (17).

Lipid Staining. Duramycin staining was performed by incubating dissected gonads from young adult worms in 0.25 μg/mL biotinylated duramycin [gift of Philip Thorpe, UT Southwestern Medical Center, Dallas (18)] and 1 μg/mL Alexa 488–streptavidin (Invitrogen) in embryonic culture medium (ECM) for 30 min. The gonads were washed twice in ECM before mounting on slides in ECM. Annexin V staining was performed by incubating dissected gonads in 1:100 Alexa 488–Annexin V (Invitrogen) for 30 min, washing in ECM twice, and mounting on slides in ECM.

Vesicle Size and Fluorescence Intensity Measurements. For the analysis of EV size in Fig. 1 and multivesicular endosome and lysosome size in Fig. S5, the perimeter of each vesicle was measured in a circle traced on TEM images by using Fiji (19). The diameter of each vesicle was calculated from the perimeter. For Fig. 2, the mean fluorescence intensity of GFP::TAT-5 was measured on the cell contact of two- and four-cell embryos in Fiji. In four-cell embryos, the cell–cell contact with the clearest plasma membrane fluorescence was measured. If the plasma membrane was not visible due to GFP::TAT-5 mislocalization, the plasma membrane was traced by using DIC. The mean intensity in the cytoplasm was then measured with the same size line in the cytoplasm of the neighboring cells. Data are presented as the ratio of the mean fluorescence on the cell contact to the neighboring cytoplasm. To measure total GFP::TAT-5 levels, two- to four-cell embryos were thresholded in Fiji to measure the integrated density in the whole embryo excluding the eggshell. As TAT-5 accumulates on EVs, all *pad-1* RNAi embryos with increased EV release where excluded from quantification. For lipid externalization measurements in Fig. 7, membranes were chosen blindly from DIC or mCh::PH images, and the mean fluorescence intensities were measured along three membranes of the same gonad by using Fiji. The three measurements were averaged to obtain the final intensity. All measurements were normalized to the vector control of the OD70 strain.

Colocalization Measurement. Embryos stained for GFP::TAT-5 and a series of endocytic markers were scored for GFP-positive cytoplasmic puncta, marker-positive puncta, and double-positive puncta for Fig. S1. Percentages are expressed in relation to the total number of GFP-positive puncta or in relation to the total number of marker-positive puncta. To measure colocalization of GFP::TAT-5 with LMP-1 or UNC-108 in Fig. 6, deconvolved and thresholded z-stacks of stained embryos were analyzed by using the colocalization tool of Imaris. Embryos used to measure colocalization with 2xFYVE in Fig. S6 where not deconvolved, because of high vesicle motility. The whole embryo excluding the eggshell was defined as the region of interest from which the Pearson's coefficient and percentage of colocalized GFP::TAT-5 voxels was calculated. The background was masked in Imaris to only measure colocalization in 2- to 12-cell embryos. The line scans in Fig. 6 were measured in Fiji by using Multi Plot with a one-pixel-width straight line or free-hand line to trace large TAT-5 vesicles. In Fig. S6, line scans were measured by using a four-pixel-width straight line or freehand line. For Fig. 6*K*, colocalization of large GFP::TAT-5 vesicles with 2xFYVE, UNC-108, or LMP-1 puncta was counted per embryo from *mon-2* mutants after *snx-6* RNAi.

Image Manipulation. For clarity, all images were cropped and rotated, and the intensity was adjusted by using Adobe Photoshop. In Figs. 4 and 6 and Fig. S5, Z-stacks were deconvolved by using Huygens Professional compute engine (Version 17.04.op5 64b). Three Zs are projected in Fig. S5; only one Z is shown in all other figures.

Statistics. The box and whisker plots in Figs. 2 and 6 were generated by using Microsoft Excel, with the lower quartile and upper quartile separated by the median. Whiskers represent the lowest and highest values, with the exception of outliers depicted with a circle. Outliers represent values above or below 1.5 times the width of the interquartile range. Error bars display SEM in Fig. 6 and Fig S6 and SD in Fig. S2. For all statistical analyses, Student's one-tailed *t* test was used with Bonferroni correction to adjust for multiple comparisons, except for the categorization of TAT-5 localization in Fig. 2*J*, which was analyzed by using Fisher's exact test (two-tailed, 2 × 3) with Bonferroni correction.

1. Fazeli G, Trinkwalder M, Irmisch L, Wehman AM (2016) *C. elegans* midbodies are released, phagocytosed and undergo LC3-dependent degradation independent of macroautophagy. *J Cell Sci* 129:3721–3731.
2. Dickinson DJ, Ward JD, Reiner DJ, Goldstein B (2013) Engineering the *Caenorhabditis elegans* genome using Cas9-triggered homologous recombination. *Nat Methods* 10:1028–1034.
3. Redemann S, et al. (2011) Codon adaptation-based control of protein expression in C. elegans. *Nat Methods* 83:250–252.
4. Paix A, et al. (2014) Scalable and versatile genome editing using linear DNAs with microhomology to Cas9 Sites in *Caenorhabditis elegans*. *Genetics* 198:1347–1356.
5. Praitis V, Casey E, Collar D, Austin J (2001) Creation of low-copy integrated transgenic lines in *Caenorhabditis elegans*. *Genetics* 157:1217–1226.
6. Sarov M, et al. (2012) A genome-scale resource for in vivo tag-based protein function exploration in *C. elegans*. *Cell* 150:855–866.
7. Fraser AG, et al. (2000) Functional genomic analysis of *C. elegans* chromosome I by systematic RNA interference. *Nature* 408:325–330.
8. Wehman AM, Poggioli C, Schweinsberg P, Grant BD, Nance J (2011) The P4-ATPase TAT-5 inhibits the budding of extracellular vesicles in *C. elegans* embryos. *Curr Biol* 21:1951–1959.
9. Kaltdorf KV, et al. (2017) FIJI macro 3D ART VeSElecT: 3D automated reconstruction tool for vesicle structures of electron tomograms. *PLoS Comput Biol* 13:e1005317.
10. Mastronarde DN (2005) Automated electron microscope tomography using robust prediction of specimen movements. *J Struct Biol* 152:36–51.
11. Kremer JR, Mastronarde DN, McIntosh JR (1996) Computer visualization of three-dimensional image data using IMOD. *J Struct Biol* 116:71–76.
12. Jantsch-Plunger V, Glotzer M (1999) Depletion of syntaxins in the early *Caenorhabditis elegans* embryo reveals a role for membrane fusion events in cytokinesis. *Curr Biol* 9: 738–745.
13. Sato M, et al. (2005) *Caenorhabditis elegans* RME-6 is a novel regulator of RAB-5 at the clathrin-coated pit. *Nat Cell Biol* 7:559–569.
14. Zhang Y, Grant B, Hirsh D (2001) RME-8, a conserved J-domain protein, is required for endocytosis in *Caenorhabditis elegans*. *Mol Biol Cell* 12:2011–2021.
15. Roudier N, Lefebvre C, Legouis R (2005) CeVPS-27 is an endosomal protein required for the molting and the endocytic trafficking of the low-density lipoprotein receptor-related protein 1 in *Caenorhabditis elegans*. *Traffic* 6:695–705.
16. Michelet X, et al. (2009) The ESCRT-III protein CeVPS-32 is enriched in domains distinct from CeVPS-27 and CeVPS-23 at the endosomal membrane of epithelial cells. *Biol Cell* 101:599–615.
17. Hadwiger G, Dour S, Arur S, Fox P, Nonet ML (2010) A monoclonal antibody toolkit for *C. elegans*. *PLoS One* 5:e10161.
18. Stafford JH, Thorpe PE (2011) Increased exposure of phosphatidylethanolamine on the surface of tumor vascular endothelium. *Neoplasia* 13:299–308.
19. Schindelin J, et al. (2012) Fiji: An open-source platform for biological-image analysis. *Nat Methods* 9:676–682.

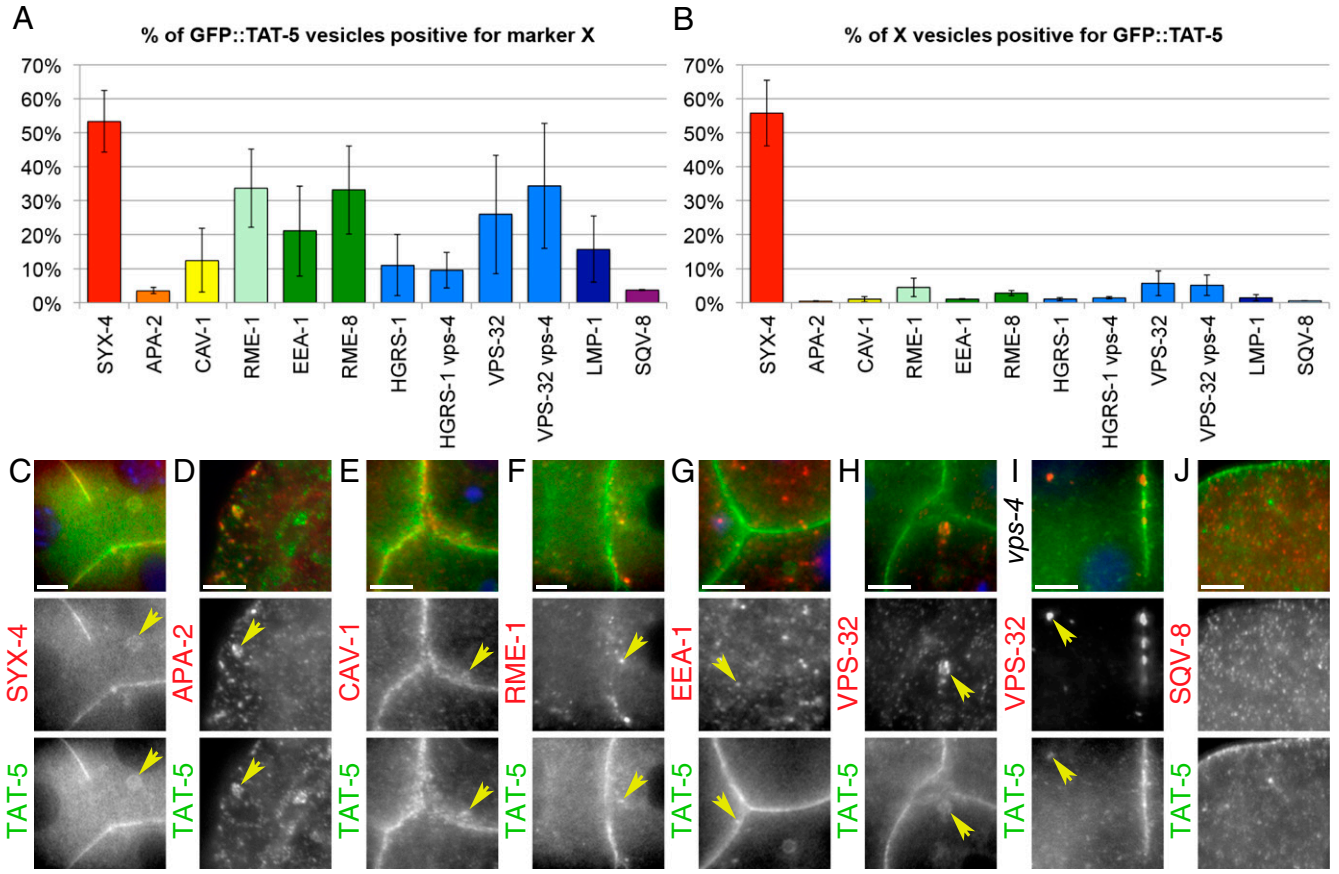

Fig. S1. GFP::TAT-5 localizes to the plasma membrane and diverse intracellular compartments. (*A* and *B*) In addition to the plasma membrane, TAT-5 labels a subset of endomembranes, including clathrin-coated vesicles, recycling endosomes, and MVBs. Histograms of colocalization frequencies of endosome and Golgi markers with GFP::TAT-5 in intracellular puncta (SYX-4: $n = 14$; APA-2: $n = 16$; CAV-1: $n = 5$; RME-1: $n = 16$; EEA-1: $n = 19$; RME-8: $n = 10$; ESCRT-0 protein HGRS-1: $n = 23$; HGRS-1 in *vps-4* RNAi: $n = 17$; VPS-32: $n = 8$; VPS-32 in *vps-4* RNAi: $n = 11$; LMP-1: $n = 19$; and SQV-8: $n = 8$ embryos). (*C*–*J*) Costaining of GFP::TAT-5 (green) with DAPI in DNA (blue) and marker proteins (red), including plasma membrane syntaxin SYX-4 in a four-cell embryo (*C*), plasma membrane-associated clathrin adaptor protein APA-2 in a meiosis II stage zygote (*D*), caveolin CAV-1 in a four-cell embryo (*E*), recycling endosome protein RME-1 in a two-cell embryo (*F*), early endosome antigen EEA-1 in a four-cell embryo (*G*), ESCRT-III component VPS-32 found in a phagosome in a four-cell wild-type embryo (*H*), and in MVBs and at the plasma membrane in a two-cell *vps-4* RNAi-treated embryo (*I*). Arrowheads indicate colocalized vesicles. (*J*) Unlike yeast Neo1p, GFP::TAT-5 rarely colocalized with the Golgi marker SQV-8, here shown in a zygote. (Scale bars: 5 μm.)

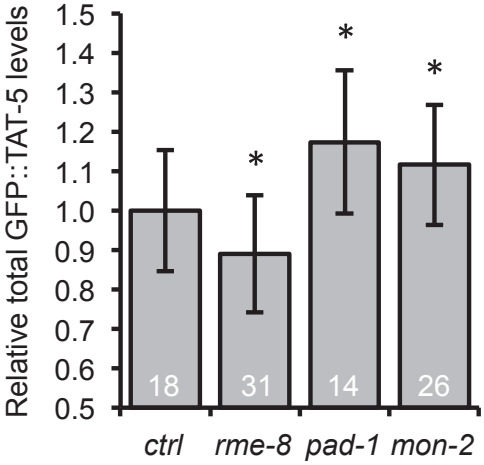

Fig. S2. GFP::TAT-5 levels are decreased after *rme-8* RNAi and increased after *mon-2* or *pad-1* RNAi. Total GFP::TAT-5 fluorescence measured from two- to four-cell control and RNAi-treated embryos is shown. TAT-5 levels are significantly decreased after *rme-8* RNAi treatment. TAT-5 levels are significantly increased in *pad-1* or *mon-2* RNAi. Student's *t* test was used for statistical analysis. $*P < 0.05$. Number of embryos scored is indicated for each genotype.

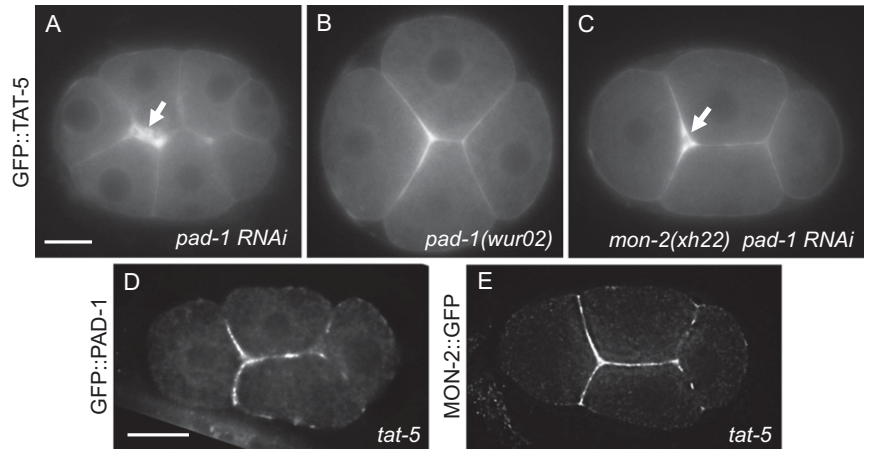

Fig. S3. TAT-5, PAD-1, and MON-2 are released in EVs. (*A*) GFP::TAT-5 is in the plasma membrane and released on EVs (arrow) in an eight-cell embryo treated with *pad-1* RNAi. (*B*) GFP::TAT-5 still localizes to the plasma membrane in a four-cell *pad-1(wur02)* maternal-zygotic deletion mutant embryo. (*C*) GFP::TAT-5 is in the plasma membrane and released on EVs (arrow) in a four-cell *mon-2(xh22)* mutant treated with *pad-1* RNAi, indicating that MON-2 and PAD-1 do not redundantly regulate TAT-5 localization. (*D* and *E*) GFP::PAD-1 and MON-2::GFP::3xFlag are increased at the cell surface after *tat-5* RNAi treatment in four-cell embryos, suggesting that cortical PAD-1 and cortical MON-2 are released outside cells in EVs. [Scale bars: *A*, 10 μm (also applies to *B* and *C*); *D*, 10 μm (also applies to *E*).]

Fig. S4. The N terminus of the essential subclass of P4-ATPases is divergent. Clustal Omega alignment of N-terminal protein fragments from *Leishmania donovani* APLT1, *Schizosaccharomyces pombe* SPAC6C3.06C, *Saccharomyces cerevisiae* Neo1p, *C. elegans* TAT-5a, *Drosophila melanogaster* CG31729-PA, and *Homo sapiens* ATP9A shows divergence in the cytosolic sequence before the first two transmembrane domains (underlined). The Snx3p-binding FEM domain (red) identified in Dalton et al., 2017 (1) is not conserved in animals.

1. Dalton LE, Bean BDM, Davey M, Conibear E (2017) Quantitative high-content imaging identifies novel regulators of Neo1 trafficking at endosomes. *Mol Biol Cell* 28:1539–1550.

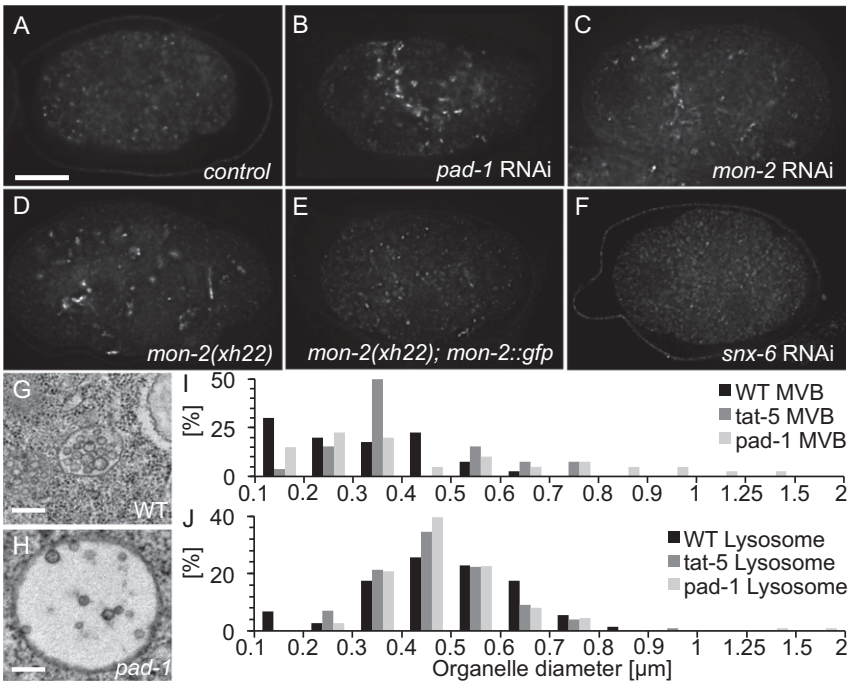

Fig. S5. Late endosomes are enlarged in *mon-2* and *pad-1* mutants. (*A*) Antibody staining shows small LMP-1–positive late endosomes or lysosomes in four-cell control embryos. (*B–D*) LMP-1–positive vesicles are enlarged after *mon-2* knockdown, in *mon-2*(*xh22*) nonsense mutants, and *pad-1* knockdown embryos. (*E*) The enlarged LMP-1–positive vesicles are rescued when MON-2::GFP::3xFlag is introduced into *mon-2(xh22)* mutants, showing that the MON-2::GFP::3xFlag reporter is functional. (*F*) LMP-1–positive vesicles are not enlarged after *snx-6* knockdown. (*G–I*) Multivesicular bodies (MVB) are significantly enlarged after *pad-1* knockdown, as shown by electron micrographs and a histogram of MVB diameter ($n = 40$ MVBs from 5 N2 and *pad-1* RNAi-treated embryos, $P < 0.01$; $n = 26$ MVBs from *tat-5* RNAi-treated embryos, $P < 0.05$). (*J*) Electron-dense lysosomes are not enlarged after *pad-1* knockdown, as shown by a histogram of lysosome diameter ($n > 70$ lysosomes from 5 N2, *pad-1* RNAi, and tat-5 RNAi embryos, $P > 0.05$). Student's *t* test was used for statistical analysis. [Scale bars: *A*, 10 μm (also applies to *B–F*); *G* and *H*, 200 nm.]

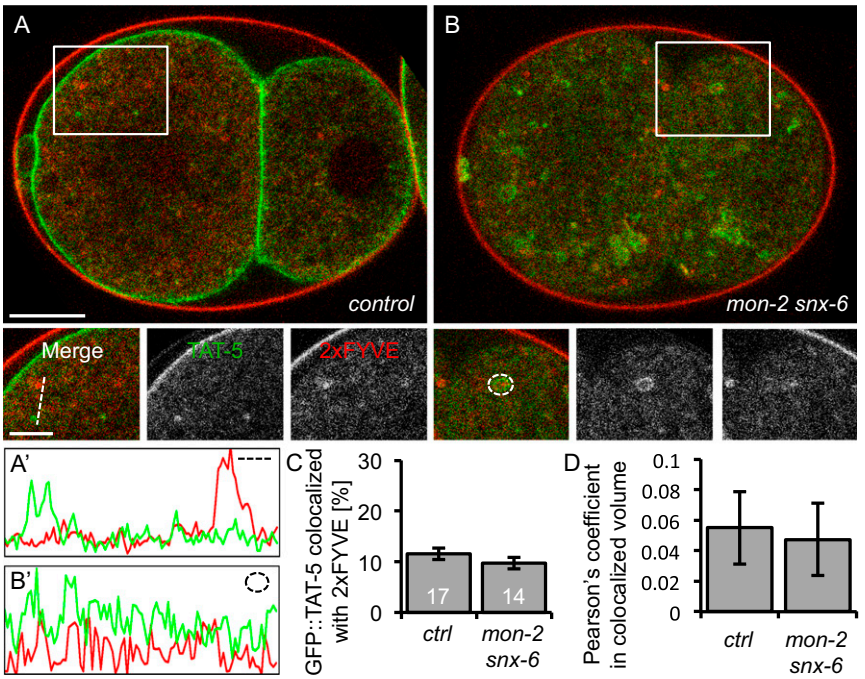

Fig. S6. GFP::TAT-5 does not accumulate in early endosomes in *mon-2 snx-6* mutants. (*A*) Confocal images of GFP::TAT-5 localizing primarily to the plasma membrane in a live two-cell control embryo. TAT-5 is also found on cytoplasmic vesicles, but they do not often colocalize with mCherry::2xFYVE, as shown in *Insets*. (*B*) Mislocalization of TAT-5 to large vesicles in *mon-2* mutants treated with *snx-6* RNAi does not increase colocalization with 2xFYVE. (*A′* and *B′*) Line scans of GFP::TAT-5 and 2xFYVE intensity next to the dotted lines or circle in *Insets*. (*C*) The percentage of TAT-5 colocalized with 2xFYVE is not increased in 2- to 12-cell *mon-2* mutant embryos after *snx-6* RNAi compared with control embryos (ctrl). Number of embryos scored is indicated for each genotype. (*D*) The Pearson's coefficient of GFP::TAT-5 colocalization with 2xFYVE does not change in *mon-2(xh22)* mutants treated with *snx-6* RNAi. [Scale bars: *A*, 10 μm (also applies to *B*); *Insets* in *A*, 5 μm (also applies to *Insets* in *B*).]

Table S1. Genetic interactions of double retromer mutants

	RNAi								
Genotype	*Ctrl*	*vps-26*	*vps-29*	*vps-35*	*snx-1*	*snx-3*	*snx-6*	*lst-4*	*mon-2*
+	—	—	—	—	—	—	—	—	—
vps-26Δ/+	—	n/a	—	Ste	Egl	—	Emb	—	n/a
vps-26Δ	Egl	Egl	Let, Egl, Ste	Let, Egl, Ste, Emb	Let, Egl, Ste	Egl, Ste, Emb	n/a	n/a	Let, Egl
vps-35Δ	Egl, Ste	Egl, Ste	Let, Egl, Ste	n/a	Let, Egl, Ste	Ste	Egl, Ste	Egl, Ste	n/a
snx-1Δ	—	Egl	—	Let, Ste	n/a	—	—	—	n/a
snx-3Δ	Egl	Let, Egl, Ste	Let, Egl, Ste	Let, Egl, Ste	Let, Ste, Egl, Emb	n/a	Egl, Emb	Egl	Egl, Emb
snx-6Δ	—	—	—	Let, Ste	—	Egl	n/a	—	n/a
lst-4Δ	—	Ste	—	Ste	—	n/a	—	n/a	n/a
mon-2(-)	—	Egl, Ste	Egl, Ste	Let, Egl, Ste	Egl, Emb	Emb	Ste, Emb	—	—

Lethal (Let), egg-laying-defective (Egl), sterile (Ste), and embryonic lethal (Emb) phenotypes were detected after knockdown with retromer RNAi in retromer deletion mutants (Δ). Synthetic phenotypes were also obtained using a heterozygous *vps-26* deletion strain (Δ/+) or a *mon-2* nonsense allele (-). These phenotypes were not detected (—) in treated wild-type (+) reporter strains or in untreated mutants, except that untreated *vps-26*, *vps-35*, and *snx-3* mutants showed an egg-laying defect. Untreated *vps-35* mutants were also partially sterile. Ctrl, control; n/a, genetic interaction not tested.

Table S2. Strains used in this study

Strain	Genotype	Source
N2	Wild type	Brenner (1)
DH1206	*rme-8(b1023) I*	Zhang et al. (2)
EU1436	*pie-1::mCherry::HistoneH2B; pie-1::GFP::tubulin; him-?*	Gift of Bruce Bowerman, University of Oregon, Eugene, OR
EW0015	*tat-1(kr15:Mos) III*	Ruaud et al. (3)
FT1091	*unc-119(ed3) III; xnIs390[pie-1::GFP::ZF1::PH(PLC1delta1), unc-119(+)]*	Bombardment
FT207	*tat-5(tm1741) II/hT2[bli-4(e937) let-?(q782) qIs48] (I; III)*	Wehman et al. (4)
FT915	*chat-1(ok1681)/nT1[qIs51] IV; pwIs834[pID3.01-tat-5a: pie-1::gfp::tat-5a, unc-119(+)]/nT1 V*	Crossed RT2277 and VC1258
FT921	*chat-1(ok1681)/nT1[qIs51] IV; +/nT1 V; W03G11.2+T01H10.1(ok2574) X*	Crossed RB1957 and VC1258
FX00847	*snx-1(tm847) X*	Shi et al. (5)
FX01595	*snx-3(tm1595) I*	Harterink et al. (6)
FX02423	*lst-4(tm2423) IV*	Chen et al. (7)
FX14884	*vps-26(tm1523) IV/nT1[qIs51?] (IV; V)*	Chen et al. (7)
FX168114	*snx-6(tm3790) V*	Chen et al. (7)
HT1593	*unc-119(ed3) III*	Dickinson et al. (8)
KN555	*vps-35(hu68) II*	Harterink et al. (6)
MCP6	*pad-1(babIs1[GFP]) I*	CRISPR/Cas9
OD58	*ltIs38[pie-1::GFP::PH(PLC1delta1), unc-119(+)] unc-119(ed3) III*	Audhya et al. (9)
OD70	*unc-119(ed3) III; ltIs44[pie-1p::mCherry::PH(PLC1delta1), unc-119(+)] V*	Kachur et al. (10)
RB1957	*W03G11.2+T01H10.1(ok2574) X*	*C. elegans* Gene KO Consortium
RT2277	*unc-119(ed3) III; pwIs834[pID3.01-tat-5a: pie-1::gfp::tat-5a, unc-119(+)] V*	Wehman et al. (4)
VC1258	*chat-1(ok1681) IV/nT1[qIs51(myo-2::GFP; pes-10::GFP; F22B7.9::GFP)](IV;V)*	*C. elegans* Gene KO Consortium
WEH02	*ltIs38[pie-1::GFP::PH(PLC1∂1), unc-119(+)] xnIs8[pJN343: nmy-2::NMY-2::mCherry, unc-119(+)] unc-119(ed3) III*	Fazeli et al. (11)
WEH03	*ltIs38[pie-1::GFP::PH(PLC1∂1), unc-119(+)] xnIs8[pJN343: nmy-2::NMY-2::mCherry, unc-119(+)] unc-119(ed3) III; bec-1(ok691) IV/nT1[qIs51] (IV; V)*	Fazeli et al. (11)
WEH14	*unc-119(ed3) III; wurIs09[mon-2::TY1::GFP::3xFLAG fosmid WRM06 12A_D10]*	Bombardment
WEH51	*unc-119(ed3) III; xnIs65[nmy-2::gfp::zf1, unc-119(+)] IV; ltIs44[pie-1p::mCherry::PH(PLC1∂1), unc-119(+)] V*	Fazeli et al. (11)
WEH69	*bec-1(ok691) xnIs65[nmy-2::gfp::zf1, unc-119(+)]/nT1 IV; ltIs44[pie-1p::mCherry::PH(PLC1delta1), unc-119(+)]/nT1[qIs51] V*	Fazeli et al. (11)
WEH73	*vps-34(h510) dpy-5(e61) I; unc-119(ed3) III; xnIs65[nmy-2::gfp::zf1, unc-119(+)] IV; ltIs44[pie-1p::mCherry::PH(PLC1delta1)] V; enEx441[vps-34(+), ced-1C::mRFP]*	Fazeli et al. (11)
WEH95	*unc-119(ed3) III; pie-1::mCherry::HistoneH2B; xnIs390[pie-1::GFP::ZF1::PH(PLC1delta1), unc-119(+)]*	Crossed EU1436 and FT1091
WEH106	*zbIs2[pie-1::LifeAct::RFP, unc-119(+)] I; bec-1(ok691) zuIs45[nmy-2::NMY-2::GFP, unc-119(+)] IV/nT1[qIs51] (IV; V)*	Fazeli et al. (11)
WEH126	*+/hT2[bli-4(e937) let-?(q782) qIs48] (I;III)*	Crossed FT207 and N2
WEH159	*pad-1(wur02) II/hT2[bli-4(e937) let-?(q782) qIs48] (I; III)*	CRISPR/Cas9
WEH192	*pad-1(wur02) II/hT2[bli-4(e937) let-?(q782) qIs48] (I; III); pwIs834[pID3.01-tat-5a: pie-1::gfp::tat-5a, unc-119(+)] V*	Crossed RT2277 and WEH159
WEH226	*rme-8(b1023) I; pwIs834[pID3.01-tat-5a: pie-1::gfp::tat-5a, unc-119(+)] V*	Crossed DH1206 and RT2277
WEH244	*unc-119(ed3) III; mon-2(xh22) IV; wurIs09[mon-2::TY1::GFP::3xFLAG fosmid WRM06 12A_D10]*	Crossed WEH14 and XH2006
WEH260	*unc-119(ed3) III; wurIs90[pGF7:pie-1::mCh::PH::ZF1, unc-119(+)]*	Bombardment
WEH263	*unc-119(ed3) III; mon-2(xh22) IV; ltIs44[pie-1p::mCherry::PH(PLC1delta1), unc-119(+)] V*	Crossed OD70 and XH2006
WEH280	*vps-26(tm1523) IV; pwIs834[pID3.01-tat-5a: pie-1::gfp::tat-5a, unc-119(+)] V*	Crossed FX14884 and RT2277
WEH281	*unc-119(ed3) III; mon-2(xh22) IV; pwIs834[pID3.01-tat-5a: pie-1::gfp::tat-5a, unc-119(+)] V*	Crossed RT2277 and XH2006
WEH310	*unc-119(ed3) III; pwIs834[pID3.01-tat-5a: pie-1::gfp::tat-5a, unc-119(+)] V; snx-1(tm847) X*	Crossed RT2277 and FX00847
WEH315	*unc-119(ed3) III; wurIs111[pGF14: pie-1p::mCherry::unc-108, unc-119(+)]*	Bombardment
WEH316	*snx-3(tm1595) I; unc-119(ed3) III; wurIs90[pGF7: pie-1::mCh::PH::ZF1, unc-119(+)]*	Crossed FX01595 and WEH260
WEH327	*unc-119(ed3) III; wurIs117[pie-1::mCh::2xFYVE, unc-119(+)]*	Bombardment
WEH329	*unc-119(ed3) III; pwIs834[pID3.01-tat-5a: pie-1::gfp::tat-5a, unc-119(+)] V; wurIs111[pGF14: pie-1p::mCherry::unc-108, unc-119(+)]*	Crossed WEH315 and RT2277
WEH330	*unc-119(ed3) III; pwIs834[pID3.01-tat-5a: pie-1::gfp::tat-5a, unc-119(+)] V; wurIs117[pie-1::mCh::2xFYVE, unc-119(+)]*	Crossed WEH327 and RT2277
WEH332	*snx-3(tm1595) I, unc-119(ed3) III; pwIs834[pID3.01-tat-5a: pie-1::gfp::tat-5a, unc-119(+)] V*	Crossed FX01595 and RT2277
WEH334	*unc-119(ed3) III; mon-2(xh22) IV; pwIs834[pID3.01-tat-5a: pie-1::gfp::tat-5a, unc-119(+)] V; wurIs111[pGF14: pie-1p::mCherry::unc-108, unc-119(+)]*	Crossed WEH281 and WEH315
XH2006	*mon-2(xh22) IV; wIs51[scm::gfp] V*	Kanamori et al. (12)

1. Brenner S (1974) The genetics of *Caenorhabditis elegans. Genetics* 77:71–94.
2. Zhang Y, Grant B, Hirsh D (2001) RME-8, a conserved J-domain protein, is required for endocytosis in *Caenorhabditis elegans. Mol Biol Cell* 12:2011–2021.
3. Ruaud A-F, et al. (2009) The *C. elegans* P4-ATPase TAT-1 regulates lysosome biogenesis and endocytosis. *Traffic* 10:88–100.
4. Wehman AM, Poggioli C, Schweinsberg P, Grant BD, Nance J (2011) The P4-ATPase TAT-5 inhibits the budding of extracellular vesicles in *C. elegans* embryos. *Curr Biol* 21:1951–1959.
5. Shi A, et al. (2009) Regulation of endosomal clathrin and retromer-mediated endosome to Golgi retrograde transport by the J-domain protein RME-8. *EMBO J* 28:3290–3302.
6. Harterink M, et al. (2011) A SNX3-dependent retromer pathway mediates retrograde transport of the Wnt sorting receptor Wntless and is required for Wnt secretion. *Nat Cell Biol* 13: 914–923.
7. Chen D, et al. (2010) Retromer is required for apoptotic cell clearance by phagocytic receptor recycling. *Science* 327:1261–1264.
8. Dickinson DJ, Ward JD, Reiner DJ, Goldstein B (2013) Engineering the *Caenorhabditis elegans* genome using Cas9-triggered homologous recombination. *Nat Methods* 10:1028–1034.
9. Audhya A, et al. (2005) A complex containing the Sm protein CAR-1 and the RNA helicase CGH-1 is required for embryonic cytokinesis in *Caenorhabditis elegans. J Cell Biol* 171:267–279.
10. Kachur TM, Audhya A, Pilgrim DB (2008) UNC-45 is required for NMY-2 contractile function in early embryonic polarity establishment and germline cellularization in *C. elegans. Dev Biol* 314:287–299.
11. Fazeli G, Trinkwalder M, Irmisch L, Wehman AM (2016) *C. elegans* midbodies are released, phagocytosed and undergo LC3-dependent degradation independent of macroautophagy. *J Cell Sci* 129:3721–3731.
12. Kanamori T, et al. (2008) β-catenin asymmetry is regulated by PLA1 and retrograde traffic in *C. elegans* stem cell divisions. *EMBO J* 27:1647–1657.

Table S3. Primers used in this study

Primer name	Sequence
pad-1 ATG sgRNA2	AAATGGCATCAGCATCAGGgttttagagctagaaatagcaagt
pad-1 Stop sgRNA1	GCCGTGGCCCGACTCGAATgttttagagctagaaatagcaagt
pad-1 Stop sgRNA6	CTCGAATCGGCTCTCTACGgttttagagctagaaatagcaagt
attB ATG coPH	aaaaagcaggcttcATGCACGGACTCCAAGACGA
attB Stop coZF1	agaaagctgggttttatCtTGGGACACGGAGCTCGTCTT
attB ATG rab-2	aaaaagcaggcttcATGTCATATGCCTACCTTTTCAAGT
attB STOP rab-2	agaaagctgggTTAACAGCATCCAGATCCACCG
attB MCS 2xFYVE	aaaaagcaggcttcAGCCCACAAGCTTTGGAATTCA
attB Stop 2xFYVE	agaaagctgggttaGTATGGCCGGCTAGCTTTCT
attB1	ggggacaagtttgtacaaaaaagcaggct
attB2	ggggaccactttgtacaagaaagctgggt
rme-8 F	GCGATGAAGGAGAAGTTTGACCA
rme-8 R	CCTGTATTAATCTCGTTCGGCTGAT
oMCP039F	aaagaaaaattgcagaaagaaataagaaATGAGTAAAGGAGAAGAACTTTTC
oMCP040R	gccgctggtacatctgcacctgatgctgatgcTTTGTATAGTTCATCCATGC
oMCP041R	gtatgcacgatatttactatctttttctcgagccgctggtacatctgcacc

Other Supporting Information Files

Dataset S1 (XLSX)